# Heterodyne Frequency Modulation in Photoinduced Force Microscopy

J. Yamanishi, Y. Naitoh, Y. J. Li, and Y. Sugawara*

*Department of Applied Physics, Osaka University, 2-1 Yamadaoka, Suita, Osaka 565-0871, Japan*

(Received 21 August 2017; revised manuscript received 12 December 2017; published 27 February 2018)

In photoinduced force microscopy (PIFM), amplitude modulation techniques, such as direct mode, and heterodyne amplitude modulation techniques have been used to detect the photoinduced force. These amplitude modulation techniques are affected by other forces because the resonance frequency shifts and nonconservative force damp the cantilever motion. Here, we investigate and propose the heterodyne-frequency-modulation (heterodyne-FM) technique for inhibiting the influence of the other forces and photothermal force. Heterodyne-FM PIFM enables the acquisition of PIFM images and force spectra without those artifacts.

DOI: 10.1103/PhysRevApplied.9.024031

## I. INTRODUCTION

Atomic force microscopy (AFM) is applied to perform nanometer-scale or atomic-scale imaging and spectroscopy of chemical [1,2], electrostatic [3,4], and magnetic [5–7] properties on material surfaces by detecting the interactions. AFM is used also for local optical spectroscopy such as near-field scanning optical microscopy [8] and tip-enhanced Raman spectroscopy [9], although these techniques measure the optical properties of the sample surface using a photodetector in the far-field, not tip-sample interaction.

Photoinduced force microscopy is a promising technique for realizing optical imaging with nanometer-scale spatial resolution [10]. This technique involves the detection of the photoinduced force between the metal tip and the sample generated by focusing light on those structures. Using this technique, the optical imaging of linear and nonlinear [11] optical effects, the plasmonic structure [12], and the time-resolved response [13] have been observed under ambient, and ultrahigh vacuum (UHV) conditions [14]. Photoinduced forces are classified into two types, scattering force and gradient force [15,16]. The scattering force originates from the momentum variation of photons. Basically, scattered light is not dependent on the tip-sample distance. Therefore, the scattering force is not attributed to high-resolution imaging of a nanometer scale. On the other hand, the gradient force is generated by the gradient of an electric field around the metal tip [15]. The electric field is constructed by the mutual interaction induced by light between the metal tip and the sample, usually considered as the dipole-dipole interaction. The gradient force reflects the optical property of the sample, which is the real part of polarizability [16]. As a result, the detection of the gradient force realizes high-resolution optical imaging.

To measure the gradient force predominantly, sideband detection, which is also called a heterodyne technique in other research, is performed instead of the direct mode [14,17,18]. Hereafter, we term this the heterodyne-amplitude-modulation (heterodyne-AM) technique in order to avoid confusion. In the direct mode, the intensity of the incident laser light is modulated at a resonance frequency of the cantilever $f_1$ ($f_2$), where $f_1$ and $f_2$ are the first and second resonance frequencies of the cantilever, respectively. Because the technique measures not the force gradient but the force, both scattering and gradient forces are detected. On the other hand, in the heterodyne-AM technique, the intensity of the incident laser light is modulated at a frequency of $f_1+f_2$ ($f_1-f_2$). The cantilever is excited at a frequency of $f_1$ ($f_2$). As a result, the mixed signal of the photoinduced force and cantilever vibration is obtained at $f_2$ ($f_1$). Since the technique detects the force gradient, the forces with larger decay lengths, such as the scattering force and the photothermal effect [14,19], can be avoided. Therefore, the heterodyne-AM technique is useful for measuring the gradient force and obtaining the optical properties of the sample.

However, in the heterodyne-AM technique, the mixed frequency, which is the sideband, does not follow $f_1$ ($f_2$). Thus, the photoinduced force signal degrades owing to other forces between the tip and the sample [18,20]. Particularly in vacuum, the $Q$ factor of the cantilever is much larger than that in the ambient environment. Hence, the degradation becomes severe. In addition, it is important to drive the cantilever at $f_1$ to prevent the jump to contact for operating noncontact AFM [1]. In that case, $f_2$ is used for the measurement of the photoinduced force, although the use of $f_2$ is less sensitive than that of $f_1$ because of the large spring constant of $f_2$. However, the measurement under vacuum condition is important to increase force sensitivity because of the high $Q$ factor of the cantilever.

*sugawara@ap.eng.osaka-u.ac.jp

 

It is realized by the absent of the ambient air or environment of low temperature. The high force sensitivity enables us to measure weak optical interactions.

In this paper, we propose a heterodyne frequency modulation (heterodyne-FM) technique that combines frequency modulation and heterodyne techniques. This technique enables us to measure the mixed force from the modulated frequency shift in frequency modulation AFM (FM AFM). The mixed force with the frequency $f_1 + f_m$ follows the shift of $f_1$ by a phase-locked loop (PLL). In addition, nonconservative forces do not affect the signal because the cantilever excitation compensates for the forces. Consequently, it is possible to extract the photoinduced force without the contribution of the other forces. Thus, the use of $f_1$ to detect the photoinduced force enhances the force sensitivity compared with that of $f_2$.

## II. METHOD

In our proposed heterodyne-FM technique, the intensity of laser light is modulated at the frequency $2f_1 + f_m$. The laser light is focused on the metal tip and sample. As a result of mixing the cantilever vibration with the frequency $f_1$, the mixed force is generated at $f_1 + f_m$ and $3f_1 + f_m$ as the gradient of the forces. The signal is detected from the frequency shift signal ($\Delta f$) of the cantilever with the frequency $f_m$. By the small amplitude approximation of the cantilever, the distance between the tip apex and the sample ($z$) is expressed as

$$\begin{aligned} z = {} & z_0 + A_1 \cos(2\pi f_1 t + \theta_1) \\ & + A_m \cos[2\pi(2f_1 + f_m)t + \theta_2] \\ & + A_{h-} \cos[2\pi(f_1 + f_m)t + \theta_{h-}] \\ & + A_{h+} \cos[2\pi(3f_1 + f_m)t + \theta_{h+}]. \end{aligned} \quad (1)$$

Here, $A_1$ is the amplitude of the cantilever excited at $f_1$. $A_m$ is that induced by the forces as a result of laser irradiation with a modulation frequency. $A_{h-}$ and $A_{h+}$ are those with mixed frequencies. $f_m$ is the difference in frequency from $2f_1$ for the heterodyne-FM technique.

When the amount of light scattered to the cantilever is markedly large, the photothermal force due to the thermal expansion of cantilever materials is induced at the modulation frequency of the laser light, $2f_1 + f_m$. It is possible that the photothermal force becomes an artifact. One of the possible artifacts is from the photothermal force modulated at $2f_1 + f_m$ that is coupled with the cantilever vibration at $f_1$. The consequent mixed signal appears at $f_1 + f_m$ as an artificial photoinduced force in the heterodyne-FM technique. Another artifact is the second derivative of forces coupling with the photothermal vibration and the cantilever vibration at $f_1 + f_m$.

These possible problems can be avoided when we additionally drive the cantilever also at $2f_1 + f_m$ to cancel the photothermal force [21], as shown in Fig. 1 [22].

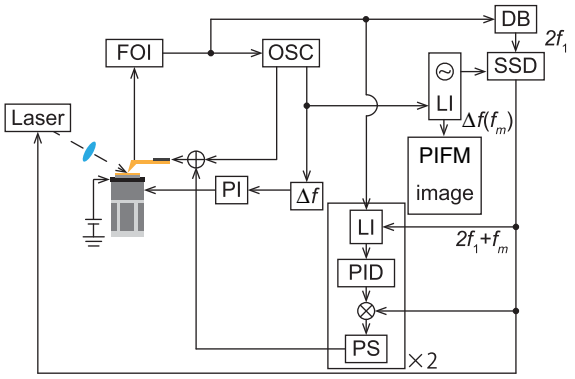


FIG. 1. Heterodyne-FM photoinduced force microscopy block diagram. The abbreviations FOI, PLL, PID, OSC, DB, SSB, LI, and PS indicate the fiber optic interferometer, phase-locked loop, PID controller, oscillation controller, doubler, single-sideband modulator, lock-in amplifier, and phase shifter, respectively. The wavelength of the laser light is 660 nm and the laser power is modulated from 0 to 50 mW. A LI detects the photoinduced force from the resonance frequency shift of the cantilever $\Delta f$ at $f_m$. The topographic image is obtained by FM AFM.

The frequency shift $\Delta f$ of the cantilever is expressed as follows by solving a point-mass spring equation [21].

$$\begin{aligned} \Delta f &\simeq -\frac{f_0}{2k}\left(\frac{dF_{\rm ts}}{dz} + \frac{dF_{\rm pif}}{dz}\cos(2\pi f_m t + \pi)\right) \\ &= \Delta f(0) + \Delta f(f_m)\cos(2\pi f_m t). \end{aligned} \quad (2)$$

The second term in Eq. (2) with the frequency $f_m$ is the photoinduced force signal in the heterodyne-FM technique. When the bandwidth of the measurement system is sufficiently broad and the delay is negligible, or the delay is compensated, the photoinduced force signal appears with the same phase or the phase delay of $\pi$ from the laser modulation signal, as shown in Eq. (2). Here, we determine the signal with the phase as the photoinduced force signal in the heterodyne-FM technique. In addition, photothermal expansion is delayed by $\pi/2$ at a high modulation frequency [23]. Therefore, the thermal expansion can be removed from the photoinduced force signal, although the photothermal expansion is negligible especially in the noncontact mode.

The equation means that the photoinduced force is approximately measured by the gradient at $z = z_0$. Thus, the long-range force such as the scattering force and the photoinduced force can be avoided [14,18]. In addition, the heterodyne-FM technique uses $f_1$ for the driving cantilever and PIFM. Therefore, it is effective in preventing the jump to contact and detecting the photoinduced force sensitively.

## III. EXPERIMENTAL SETUP

Figure 1 shows a heterodyne frequency modulation (heterodyne-FM) photoinduced force microscopy block diagram. The abbreviations in Fig. 1 namely, FOI, PLL,

PID, OSC, DB, SSB, LI, and PS indicate the fiber optic interferometer, phase-locked loop, PID controller, oscillator, doubler, single-sideband modulator, lock-in amplifier, and phase shifter, respectively. FOI detects the cantilever oscillation. From the oscillation with the frequency $f_1$, the following DB and SSB form the signal of $2f_1 + f_m$, where $f_m$ originates from the oscillator of LI1. Thus, the laser power is modulated at $2f_1 + f_m$. As a result of laser illumination, the photoinduced force is measured from $\Delta f$ as $\Delta f(f_m)$ by the lock-in $X$ signal in LI1. Two LIs, following PID, a multiplier, and a phase shifter create the additional excitation signal to suppress the photothermal vibration. Then, the additional excitation signal is added to the cantilever excitation signal. These measurements are performed at room temperature under UHV with a pressure of less than $5.0 \times 10^{-11}$ Torr. As a sample, we deposit a gold thin film of 30-nm thickness on a mica substrate [24,25]. The gold thin film is fabricated by electron beam evaporation with a heating of the substrate at 773 K. A gold-coated cantilever whose spring constant is 5 N/m, and $f_1 = 48\,(f_2 = 296)$ kHz is used. The $Q$ factors $Q_1\,(Q_2)$, of the cantilever at $f_1\,(f_2)$ are 10 537 (8056), respectively, and $f_m = 350$ Hz. The laser power is modulated from 0 to 50 mW.

## IV. RESULTS AND DISCUSSION

Figure 2 shows the suppression of the photothermal vibration at $2f_1 + f_m$. Figure 2(a) shows the power spectral density (PSD) of the cantilever illuminated by a laser without further suppression. Figure 2(b) shows that with further suppression. Without further suppression, the PSD of the photothermal vibration at $2f_1 + f_m$ is 4210 fm/$\sqrt{\text{Hz}}$. On the other hand, with further suppression, that becomes 81 fm/$\sqrt{\text{Hz}}$, with the same order as the noise density of our system. It is possible that the small rest component is due to the scattering light going through the fiber, which does not indicate the true cantilever vibration. With further suppression, it is possible to avoid the artifact as mentioned. When only the tip can be illuminated and the amount of scattered light is as small as that when using the objective lens, further suppression is not necessary. Even in our experiments, there are no significant differences observed in the force curves and images with and without further suppression. This indicates that it is not always necessary to perform further suppression because the contribution of the artifact mentioned above is sufficiently small. Hereafter, we show the results about the heterodyne-FM technique with the suppression.

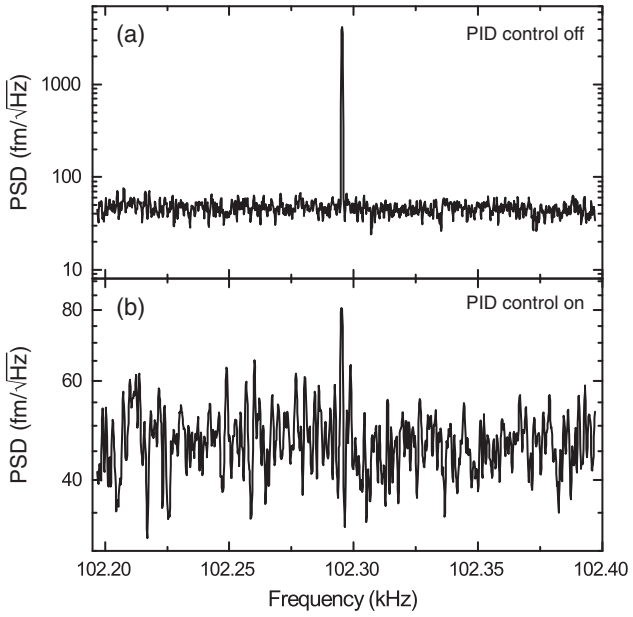


FIG. 2. Power spectral density (PSD) of the cantilever with the photothermal vibration. (a) and (b) are those without and with PID control to suppress the photothermal vibration, respectively. The laser modulation frequency is $2f_1 + f_m = 2 \times 48 + 0.35$ kHz.

Figure 3(a) shows the topography (AFM image) of the gold thin film on the mica substrate. The PIFM images obtained by heterodyne-FM, heterodyne-AM, and direct mode are shown in Figs. 3(b)–3(d), respectively. There are some depressions in the gold thin film in Fig. 3(a). Such depressions are formed during the sample preparation. In Fig. 3(b), the photoinduced force increases on the

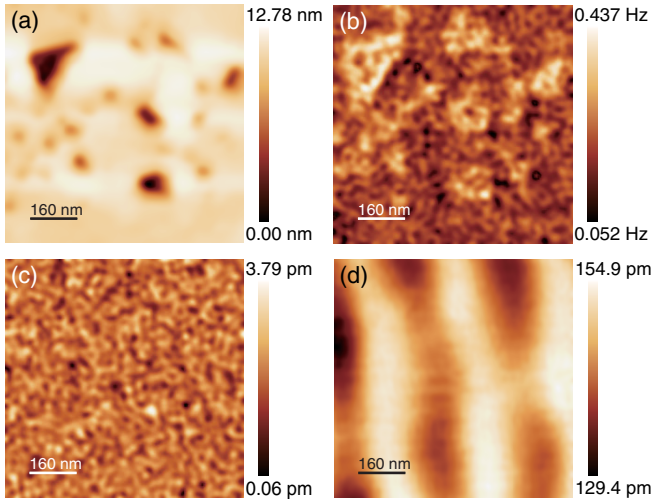


FIG. 3. Scan images. (a) Topographic image, (b) PIFM image of gold film obtained by heterodyne-FM technique, and (c) PIFM image obtained by the heterodyne-AM technique. (d) PIFM image obtained in the direct mode. Scale bars show (a) the height of the topography, (b) the modulation amplitude of the frequency shift $\Delta f(f_m)$, and (c) and (d) the amplitudes at $f_2$, $(A_2)$. Scan sizes are $800 \times 800$ nm$^2$. The amplitude at $f_1$ is 25 nm, the frequency shift is $-7.0$ Hz, the spring constant of the cantilever is 5.0 N/m, $f_1 = 48$ kHz, $f_2 = 296$ kHz, and $f_m = 350$ Hz. The $Q$ factors of the cantilever at $f_1$ and $f_2$ are 10 537 and 8056, respectively. The bandwidth of LI1 and LI2 are 20.9 and 13.1 Hz for the heterodyne-FM mode. The bandwidth for the PIFM signal in all modes is same, i.e., 20.9 Hz.

depressions because of the confined surface fields at the sharp gold edge. In this scheme, no PIFM signal is observed in the heterodyne-AM technique, as shown in Fig. 3(c), since we use $f_2$ for PIFM measurement in the heterodyne-AM technique and in the direct mode. Although the use of $f_1$ is suitable as mentioned in previous reports, $f_1$ is used in noncontact AFM to prevent the jump to contact. Therefore, the heterodyne-FM technique is superior because of the sensitiveness of the system to the difficulty in focusing the light. In the direct mode [Fig. 3(d)], the PIFM image does not reflect the structure of the surface. The interference between the cantilever and the surface appear in the image. These results indicate that the heterodyne-FM (heterodyne-AM) technique can also remove the signal of stray light going through the fiber.

Figures 4 are the force curves as a function of the tip—sample distance in the respective modulation modes. (a) is $\Delta f$ detected in FM AFM. (b)–(d) show the photoinduced force signals in the heterodyne-FM [$\Delta f(f_m)$], heterodyne-AM ($A_2$), direct mode ($A_2$), respectively. The nearest distance of the force curves is determined as 0.0 nm. When the tip-sample distance decreases, $\Delta f$ gradually decreases as shown in Fig. 4(a). In contrast, the heterodyne-FM signal is nearly 0 Hz in the range of $z =$ 3.0–10.0 nm and it increases sharply in the range of $z <$ 3.0 nm [Fig. 4(b)]. This increase is because the plasmon coupling between the tip and the sample is sharply enhanced. Figure 4(c) indicates that the heterodyne-AM technique gives no signal because of its low sensitivity, and that signal is independent of the tip-sample distance. In Fig. 4(d), the direct mode shows many artifacts from stray light going through the fiber and the photothermal force. As the tip-sample distance decreases, the artifacts become large owing to the coupling of the photothermal vibration and the other forces. Then, the signal intensity decreases because $f_2$ markedly shifts owing to the tip-sample interaction. Considering this result, the heterodyne-FM technique can inhibit the change in the PIFM signal intensity owing to the shift of the resonance frequency of the cantilever and the artifact originating from the photothermal effect.

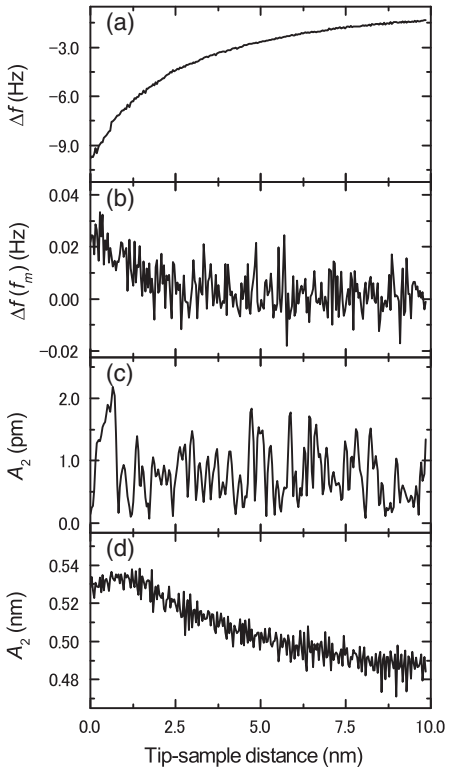


FIG. 4. Force curves of (a) $\Delta f$ in FM AFM, (b) $\Delta f(f_m)$ in the heterodyne-FM, (c) $A_2$ in the heterodyne-AM, and (d) $A_2$ in the direct mode. The parameters are the same as those in Fig. 3.

Using the heterodyne-FM technique, the minimum detectable gradient force is estimated at about 419 fN in our measurement system [21]. When this technique is performed in a low temperature, the weaker interaction can become detectable.

## V. CONCLUSION

In this article, we investigate and propose the heterodyne-FM technique. This technique enables us to obtain the photoinduced force without the artifact from the photothermal force and the change in the resonance frequency of the cantilever, and to realize true optical imaging. This technique can be used also in the tapping-mode AFM using a similar scheme without PLL. Additionally, the technique is applicable to other modulation techniques with thermal effects such as microwave and x ray. Although we also perform further PID control for the suppression of the photothermal vibration, it is not necessary even under a condition with marked scattering.

The optical responses of sample surface depend on the light frequency, and surface polaritons include information not only on geometrical structures of samples but also on electronic wave functions of excited states and ground states. Therefore, it is important to further understand observed images with theoretical analysis for the photo-induced force microscopy.

## ACKNOWLEDGMENTS

This work was supported by JSPS KAKENHI Grants No. JP16H06327, No. JP16H06504, and No. JP16K45678 in Scientific Research on Innovative Areas “Nano-Material Optical-Manipulation” and by the Photonics Advanced Research Center program of the Ministry of Education, Culture, Sports, Science and Technology.

[1] R. García and R. Perez, Dynamic atomic force microscopy methods, Surf. Sci. Rep. **47**, 197 (2002).
[2] Y. Sugimoto, P. Pou, M. Abe, P. Jelinek, R. Pérez, S. Morita, and O. Custance, Chemical identification of individual

surface atoms by atomic force microscopy, Nature (London) **446**, 64 (2007).
[3] W. Melitz, J. Shen, A. C. Kummel, and S. Lee, Kelvin probe force microscopy and its application, Surf. Sci. Rep. **66**, 1 (2011).
[4] F. Mohn, L. Gross, N. Moll, and G. Meyer, Imaging the charge distribution within a single molecule, Nat. Nanotechnol. **7**, 227 (2012).
[5] Y. Kinoshita, Y. Li, S. Yoshimura, H. Saito, and Y. Sugawara, Magnetic resonance force microscopy using ferromagnetic resonance of a magnetic tip excited by microwave transmission via a coaxial resonator, Nanotechnology **28**, 485709 (2017).
[6] F. Pielmeier and F. J. Giessibl, Spin Resolution and Evidence for Superexchange on NiO (001) Observed by Force Microscopy, Phys. Rev. Lett. **110**, 266101 (2013).
[7] J. Grenz, A. Köhler, A. Schwarz, and R. Wiesendanger, Probing the Nano-Skyrmion Lattice on Fe/Ir (111) with Magnetic Exchange Force Microscopy, Phys. Rev. Lett. **119**, 047205 (2017).
[8] F. Zenhausern, Y. Martin, and H. K. Wickramasinghe, Scanning interferometric apertureless microscopy: Optical imaging at 10 angstrom resolution, Science **269**, 1083 (1995).
[9] R. M. Stöckle, Y. D. Suh, V. Deckert, and R. Zenobi, Nanoscale chemical analysis by tip-enhanced Raman spectroscopy, Chem. Phys. Lett. **318**, 131 (2000).
[10] I. Rajapaksa, K. Uenal, and H. K. Wickramasinghe, Image force microscopy of molecular resonance: A microscope principle, Appl. Phys. Lett. **97**, 073121 (2010).
[11] I. Rajapaksa and H. K. Wickramasinghe, Raman spectroscopy and microscopy based on mechanical force detection, Appl. Phys. Lett. **99**, 161103 (2011).
[12] T. U. Tumkur, X. Yang, B. Cerjan, N. J. Halas, P. Nordlander, and I. Thomann, Photoinduced force mapping of plasmonic nanostructures, Nano Lett. **16**, 7942 (2016).
[13] J. Jahng, J. Brocious, D. A. Fishman, S. Yampolsky, D. Nowak, F. Huang, V. A. Apkarian, H. K. Wickramasinghe, and E. O. Potma, Ultrafast pump-probe force microscopy with nanoscale resolution, Appl. Phys. Lett. **106**, 083113 (2015).
[14] J. Yamanishi, Y. Naitoh, Y. J. Li, and Y. Sugawara, Heterodyne technique in photoinduced force microscopy with photothermal effect, Appl. Phys. Lett. **110**, 123102 (2017).
[15] L. Novotny and B. Hecht, *Principles of Nano-Optics* (Cambridge University Press, Cambridge, 2012).
[16] J. Jahng, J. Brocious, D. A. Fishman, F. Huang, X. Li, V. A. Tamma, H. K. Wickramasinghe, and E. O. Potma, Gradient and scattering forces in photoinduced force microscopy, Phys. Rev. B **90**, 155417 (2014).
[17] Z. M. Ma, L. Kou, Y. Naitoh, Y. J. Li, and Y. Sugawara, The stray capacitance effect in Kelvin probe force microscopy using FM, AM and heterodyne AM modes, Nanotechnology **24**, 225701 (2013).
[18] J. Jahng, B. Kim, E. S. Lee, and E. O. Potma, Quantitative analysis of sideband coupling in photoinduced force microscopy, Phys. Rev. B **94**, 195407 (2016).
[19] N. Umeda, S. Ishizaki, and H. Uwai, Scanning attractive force microscope using photothermal vibration, J. Vac. Sci. Technol. B **9**, 1318 (1991).
[20] D. C. Kohlgraf-Owens, S. Sukhov, L. Greusard, W. Y. De, and A. Dogariu, Optically induced forces in scanning probe microscopy, Nanophotonics **3**, 105 (2014).
[21] See Supplemental Material at http://link.aps.org/supplemental/10.1103/PhysRevApplied.9.024031 for the detailed deviation of Eq. (2), and the minimum detectable force in the heterodyne-FM technique.
[22] T. R. Rodrıguez and R. García, Theory of Q control in atomic force microscopy, Appl. Phys. Lett. **82**, 4821 (2003).
[23] D. Ma, J. L. Garrett, and J. N. Munday, Quantitative measurement of radiation pressure on a microcantilever in ambient environment, Appl. Phys. Lett. **106**, 091107 (2015).
[24] S. Buchholz, H. Fuchs, and J. P. Rabe, Surface structure of thin metallic films on mica as seen by scanning tunneling microscopy, scanning electron microscopy, and low-energy electron diffraction, J. Vac. Sci. Technol. B **9**, 857 (1991).
[25] B. Lüssem, S. Karthäuser, H. Haselier, and R. Waser, The origin of faceting of ultraflat gold films epitaxially grown on mica, Appl. Surf. Sci. **249**, 197 (2005).